Development 139, 2935-2944 (2012) doi:10.1242/dev.081471

Multiscale mechanisms of cell migration during development: theory and experiment

Rebecca McLennan[1,*], Louise Dyson[2,*], Katherine W. Prather[1], Jason A. Morrison[1], Ruth E. Baker[2], Philip K. Maini[2,3] and Paul M. Kulesa[1,4,‡]

SUMMARY

Long-distance cell migration is an important feature of embryonic development, adult morphogenesis and cancer, yet the mechanisms that drive subpopulations of cells to distinct targets are poorly understood. Here, we use the embryonic neural crest (NC) in tandem with theoretical studies to evaluate model mechanisms of long-distance cell migration. We find that a simple chemotaxis model is insufficient to explain our experimental data. Instead, model simulations predict that NC cell migration requires leading cells to respond to long-range guidance signals and trailing cells to short-range cues in order to maintain a directed, multicellular stream. Experiments confirm differences in leading versus trailing NC cell subpopulations, manifested in unique cell orientation and gene expression patterns that respond to non-linear tissue growth of the migratory domain. Ablation experiments that delete the trailing NC cell subpopulation reveal that leading NC cells distribute all along the migratory pathway and develop a leading/trailing cellular orientation and gene expression profile that is predicted by model simulations. Transplantation experiments and model predictions that move trailing NC cells to the migratory front, or vice versa, reveal that cells adopt a gene expression profile and cell behaviors corresponding to the new position within the migratory stream. These results offer a mechanistic model in which leading cells create and respond to a cell-induced chemotactic gradient and transmit guidance information to trailing cells that use short-range signals to move in a directional manner.

KEY WORDS: Neural crest, Cranial cell migration, Chick, Laser capture microdissection, qPCR, Mathematical modeling, Numerical simulation

INTRODUCTION

Prevailing models of long-distance cell migration involve multicellular streams that are sculpted by dynamic cell-cell contacts and local inhibitory signals (Abercrombie, 1979; Teddy and Kulesa, 2004; Young et al., 2004; Druckenbrod and Epstein, 2007; Theveneau and Mayor, 2011; Darnton et al., 2010; Huang, 2009; Murase and Horwitz, 2004). In these models, cell movement is encouraged by cell-cell contact, which may be manifested as nudging from behind (Davis and Trinkaus, 1981) or the detachment of cells at the front of a migratory cell sheet (Carmona-Fontaine et al., 2008) to create space. These cell behaviors alone may not produce directional movement of a multicellular stream, but when local inhibitory signals restrict cell movements the result can be long-distance directed cell movement.

By contrast, other models suggest that cells respond to chemotactic signals that drive the directional migration of individual cells (Dormann and Weijer, 2003; Richardson and Lehmann, 2010; Tarbashevich and Raz, 2010; Kulesa et al., 2010; Roussos et al., 2011; Cai et al., 2012) or cell clusters (Valentin et al., 2007; Aman and Piotrowski, 2010; Streichan et al., 2011). In these models, cells may respond directly to a chemotactic signal or receive guidance from neighboring cells.

[1]Stowers Institute for Medical Research, 1000 East 50th St, Kansas City, MO 64110, USA. [2]Oxford University, Centre for Mathematical Biology, Mathematical Institute, University of Oxford, 24-29 St Giles', Oxford OX1 3LB, UK. [3]Oxford Centre for Integrative Systems Biology, Department of Biochemistry, University of Oxford, South Parks Road, Oxford OX1 3QU, UK. [4]Department of Anatomy and Cell Biology, University of Kansas School of Medicine, Kansas City, KS 64157, USA.

*These authors contributed equally to this work
‡Author for correspondence (pmk@stowers.org)

Accepted 25 May 2012

As long-distance cell migration is a major aspect of embryonic development (Dormann and Weijer, 2003; Richardson and Lehmann, 2010; Tarbashevich and Raz, 2010; Kulesa and Gammill, 2010), adult morphogenesis (Hatten and Roussel, 2011), tissue repair (Burns and Steinberg, 2011) and cancer metastasis (Roussos et al., 2011; Friedl and Gilmour, 2009), the examination of this phenomenon could have significant implications for better understanding birth defects and disease. Yet, even with multiscale data collected from different model systems and emerging computational models, the cellular and molecular mechanisms of long distance cell migration are still unclear. This is due in part to a disconnect between theory and experiment that limits the testing of various hypotheses parametrised by biological data. Thus, what is needed is a fully integrative experimental-modeling approach that can reject certain hypotheses in favor of others and elucidate multiscale mechanisms of cell migration.

Here, we examine how a subpopulation of embryonic cells travel long distances and respond to tissue growth to accurately reach a target. We study this question using the neural crest (NC) as our model experimental system. NC cells exit the dorsal neural tube (NT) and travel long distances throughout the developing embryo along stereotypical pathways rich in microenvironmental signals, mesoderm and extracellular matrix (Noden and Trainor, 2005; Perris and Perissinotto, 2000). The NC cell population is crucial for proper development of the face, heart and peripheral nervous systems, and is the cellular origin of the highly aggressive cancers, melanoma and neuroblastoma (Trainor, 2005; Sauka-Spengler and Bronner-Fraser, 2008; Gammill and Roffers-Agarwal, 2010; Kasemeier-Kulesa et al., 2008; Jiang et al., 2011). The recent explosion of multiscale cellular and molecular data on NC cell migration (Kulesa et al., 2010; Kulesa and Gammill, 2010;

Gammill and Roffers-Agarwal, 2010) now offers us the opportunity to move from merely descriptive to mechanistic models using an integrated approach.

In this paper, we gather new biological data and formulate a computational model of NC cell migration. We test our model hypotheses by experiment. Computational model predictions and biological experiments are carried out simultaneously, but interpreted in isolation and later compared. We first visualize cranial NC cell morphologies in living chick embryos and measure changes in cell orientation and tissue growth along a typical migratory pathway, using fluorescence cell labeling, high-resolution confocal microscopy and novel cell shape analyses. We formulate a computational model of NC cell migration and perform tissue ablation and tissue transplantation experiments, simulated in silico, that delete or move NC cells to different locations within a migratory stream. We assess changes in NC cell gene expression, using a novel laser capture microdissection (LCM) and a quantitative PCR strategy, cell orientation and cell behaviors. We refine our model hypotheses to produce a mechanistic explanation of long-distance cell migration.

MATERIALS AND METHODS

Embryos and cell labeling

Fertilized white leghorn chicken eggs (supplied by Placid Acre Poultry, Jasper, MO) were incubated at 38°C in a humidified incubator until the desired HH (Hamburger and Hamilton, 1951) stage of development, and prepared for experiments as previously described (McLennan and Kulesa, 2007). Plasmid DNA (5 μg/μl) was injected into the lumen of the neural tube at the axial level of the rostral hindbrain (HH stage 9), as previously described (McLennan and Kulesa, 2007).

Cell morphometric measurements and 3D confocal imaging

The angle of orientation (measured between 0° and 90°) was defined as the smallest angle between the long axis of the nucleus of the cell and the tangent to the migratory route (measured as the shortest distance between the cell nucleus and the migratory route). For each time point (8 hours, 16 hours and 24 hours), 200-400 NC cells (30-50 images) were analyzed. Three-dimensional image *z*-stacks were collected on an inverted laser scanning confocal microscope (LSM 510, Zeiss) using either a Plan-Neofluar 10×/0.3 (Zeiss) or a Plan-Neofluar 20×/0.8 (Zeiss). Images were manipulated using AIM software (Zeiss).

Isolation of leading and trailing NC cells and quantitative PCR (qPCR)

For flow cytometry analysis (FACs), tissue containing the rhombomere 4 (r4) NC cell migratory stream was manually dissected (lead versus trailing cell subpopulations) from embryos aged to correspond to the 24 hour time point after electroporation of HH stage 9 embryos. Between 20,000 and 54,000 cells were isolated for each subpopulation, and the isolation was performed in triplicate.

Laser capture microdissection (LCM) was performed using a Zeiss PALM Microbeam (Zeiss). NC cells of interest were identified by fluorescence, cut and catapulted without contact into an adhesive cap (415190-9181-000, Zeiss). Lysis solution (10 μl) from Taqman PreAmp Cells-to-Ct kit (4387299, Applied Biosystems/Ambion, Austin, TX, USA) was added to the tissue in each adhesive cap. A 14-cycle pre-amplification of cDNA was performed using 84 Taqman Gene Expression Assays (supplementary material Table S1), according to ABI's instructions for the Taqman PreAmp Cells-to-Ct kit, except that the reaction volumes were reduced by half. Each sample was represented by three or four biological replicates, with each biological replicate consisting of captured NC cells from one to four embryos. All samples were normalized using three reference genes whose stable expression was validated by GeNorm.

Mathematical model

We formulated a two-dimensional off-lattice individual-based model (IBM) of NC cell migration, with a continuous vascular endothelial growth factor (VEGF) density. Cells were modeled as non-overlapping circular discs and moved by sensing VEGF in a random direction at constant time intervals of 0.5 hours. Active cell movement occurred only if the VEGF gradient was favorable and there were no other cells impeding motion. The domain was modeled as a rectangle, initially 1100 μm (length) by 120 μm (width), that extended in length, analogous to a 2D representation of the chick cranial NC cell migratory pathway. Cells were carried along with the growing tissue in addition to their active migration. In the model the cell speed was 45 μm/hr and filopodial extensions were 50 μm long. Both leading and trailing cells internalized VEGF, thus creating a gradient in VEGF (supplementary material Appendix S1). In the first extension to the model, trailing cells used directional cues from leading cells. In a further extension, cells were allowed to switch between the trailing and leading phenotype, with switching dependent on the extent to which the VEGF gradient was favorable.

The model pseudocode was as follows: (1) initialize cells and VEGF; (2) if time=cell insertion time and there is space for new cells, insert new cells at x=0; (3) solve for the VEGF profile, using the current positions of cells and domain length; (4) domain grows; (5) cells move [(a) pick a cell at random from those not yet considered; (b) pick a random angle to extend a filopodium; (c) b=the integral of VEGF multiplied by a weighting function around the cell body; (d) f=the integral of VEGF multiplied by a weighting function (Fig. 3) around the end of the filopodium; (e) if f>b and there are no other cells in the way, then move in the direction of the filopodia (f) or else the NC cell remains where it is; (g) repeat steps 5(a)-5(f) until all the cells have been considered]; (6) update time by letting time=time + time step; (7) if time<end time, then repeat from step 2.

The cells were considered in a random order, using the calculated VEGF concentration to decide which direction to move in. Each cell determined the concentration of VEGF near the cell body and before a point the length of the filopodium away in a random direction, by integrating the VEGF concentration multiplied by a weighting function around these points, similar to that for the internalization of VEGF. The cell attempted to move in the direction of the filopodium if, and only if, the VEGF concentration was found to be more favorable in the region of the filopodium. If another cell was found to occupy the desired space already, or the VEGF was not favorable in the new position, then the considered cell would not actively move during this time. Although at each time step only one filopodium was examined, cells in this model moved their filopodia faster than was found experimentally, sampling many more directions than a single filopodium could in vivo. The single filopodium in our model can therefore be considered representative of the multiple filopodia that are found experimentally.

In the extension to our model, cells entering the domain later were considered to be 'trailing cells', with a different phenotype to the lead cells. This second population still internalized VEGF, but no longer responded to it. Instead, trailing cells looked for a cell that had made contact with a leading cell. Trailing cells that had not made contact were shown in red in our simulations. When the filopodium of a trailing cell intersected with a cell that had made contact with a leading cell, the trailing cell attached to the cell it had found and moved each time in the direction of that cell. Thus 'chains' of trailing cells were formed behind a leader cell, which followed the VEGF gradient. Trailing cells that were in a chain were shown in white in our simulations. If the cell in front moved out of reach of the filopodium of the trailing cell, then the cell detached and again sought another cell to follow.

In a further extension to the model, we allowed cells to move between the leading and trailing populations. In this case, cells sampled the VEGF gradient in a number of directions and trailing cells converted to leaders if the gradient was favorable in more than half of directions sampled. In our simulations, trailing cells sampled the gradient in 16 directions and converted to leaders if the gradient was favorable in more than eight directions.

RESULTS

A NC cell migratory stream has a unique cellular profile that responds to non-linear tissue growth

To determine whether NC cells exit from the dorsal neural tube with or without directional information, we examined the distribution of NC cell nuclear and cell body orientation with

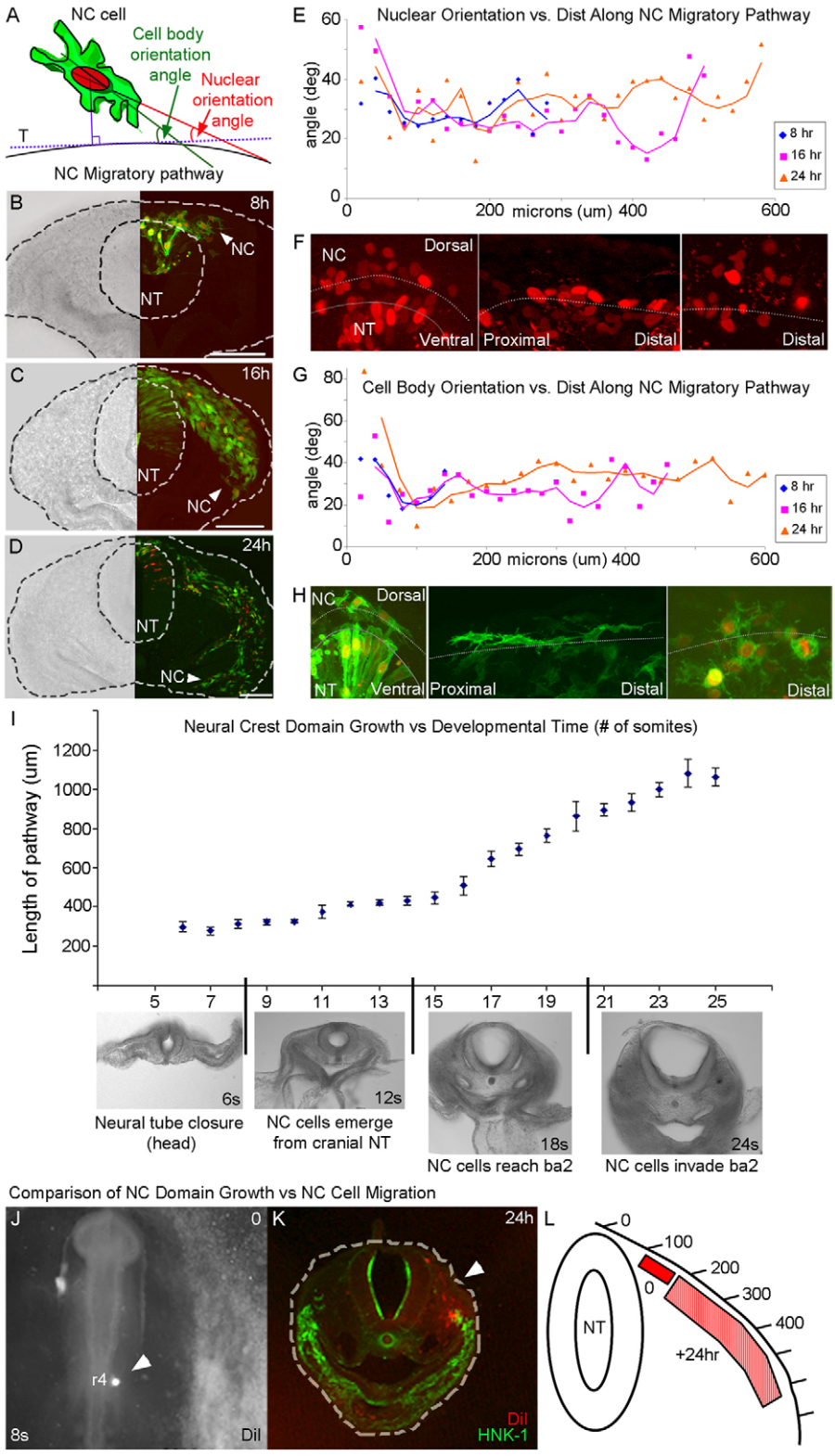

Fig. 1. NC cell direction is acquired after cells exit the neural tube and cells move faster than non-linear tissue growth. (**A**) Orientation angle measurements. (**B-D**) Typical projected images from 3D confocal *z*-stacks of transverse sections through the r4 NC cell migratory stream at 8, 16 and 24 hours after electroporation. (**E**) Average nuclear orientation angle with respect to distance along the migratory route from 8- (*n*=318 cells, 29 embryos), 16- (*n*=346 cells, 15 embryos) and 24- (*n*=240 cells, 25 embryos) hour data. (**F**) Representative images of migratory NC cells. (**G**) Average cell body orientation angle with respect to distance along the migratory route for 8- (*n*=89 cells, 10 embryos), 16- (*n*=254 cells, 27 embryos) and 24- (*n*=248 cells, 11 embryos) hour data. (**H**) Gap43-EGFP membrane-labeled NC cells. (**I**) Average length of the NC cell migratory domain at increasing developmental times. (**J**) Focal injection (arrowhead) of DiI into the lateral mesoderm prior to NC cell emigration. (**K**) Twenty four hours after injection in J. Arrowhead indicates site of injection. (**L**) Average spread of DiI-labeled tissue. Scale bars: 100 μm. NC, neural crest; NT, neural tube.

respect to the migratory pathway (Fig. 1A). In our measurements, low cell body and nuclear orientation angles correlate with high NC cell alignment to the migratory pathway (Fig. 1A). We find that NC cells emerge from the dorsal neural tube and display rounded shapes (Fig. 1B-D,H) with high orientation angles (Fig. 1E,G). That is, NC cells emerge from the neural tube without polarity or alignment to the migratory pathway. NC cells become aligned to the migratory pathway within 100-150 μm downrange from their neural tube exit (Fig. 1B-H). As more NC cells exit from the neural tube, the migratory stream develops a stereotypical cellular profile (Fig. 1B-D). Leading NC cells at the migratory front have consistently

high nuclear and cell body orientation angles, displaying less alignment to the migratory pathway (Fig. 1B-H). Trailing NC cells, located midstream, remain near (within one to two cell diameters) the migratory pathway, correlating with low cell orientation angles (Fig. 1B-H).

To determine whether this observed cellular orientation profile of the NC cell migratory stream is consistent over time, we measure embryos at 8 hours (n=39), 16 hours (n=42) and 24 hours (n=36) after electroporation (Fig. 1B,C). Measurements reveal that the NC cell migratory stream maintains a similar cellular profile over time (Fig. 1E,G). Thus, our observations of cell shape and measurements of cell orientation reveal a unique cellular profile of emerging cranial NC cells and of a typical NC cell migratory stream.

To determine growth of the NC cell migratory domain over time, we measured tissue expansion during the developmental stages of cranial NC cell migration. Measurements of the distance from the dorsal neural tube midline to the distal tip of the lateral mesoderm show that the migratory pathway lengthens non-linearly during cranial NC cell migration, according to a logistic function (Fig. 1I; supplementary material Appendix S1). At developmental stages prior to cranial NC cell exit from the hindbrain, the NC cell migratory domain lengthens at a slow linear rate (Fig. 1I; see 5-10). During the major portion of developmental time when cranial NC cells invade downrange microenvironments, the migratory domain lengthens dramatically (Fig. 1I; see 10-21). As NC cells enter the second branchial arch, lateral growth slows to zero, and the tissue length reaches an asymptotic value (Fig. 1I; see 21-25). DiI injections into the mesoderm lateral to the dorsal neural tube and separate fluorescent marking (distinct from DiI) of premigratory cranial NC cells show that NC cells move faster than the tissue growth (Fig. 1J-L). Thus, NC cells are not simply carried along by tissue growth, but move rapidly to reach peripheral targets.

A simple chemotaxis model is insufficient to explain our experimental data

We constructed a mathematical model based on our initial hypothesis that chemotaxis guides NC cells to move in a directional manner to long-distance targets (Fig. 2A). We included known NC cell biological data (reviewed by Kulesa and Gammill, 2010; Kulesa et al., 2010) and our new tissue growth measurements (Fig. 1I). We modeled NC cells on a 2D rectangular domain as off-lattice agents (Fig. 2A) that interact with vascular endothelial growth factor (VEGF). VEGF is a reasonable choice for a NC cell guidance signal as its expression has been well characterized in the chick surface ectoderm directly overlying the cranial NC cell migratory pathways (McLennan et al., 2010). In addition, VEGF has been shown to induce NC cells to move chemotactically both in vitro and in vivo into typical inhibitory NC cell free zones (McLennan et al., 2010).

In our model, the concentration of VEGF is governed by a partial differential equation that describes its diffusion, uptake and production (supplementary material Appendix S1). We initially assume a homogeneous production of VEGF in the NC microenvironment, as VEGF expression is uniform in the surface ectoderm overlying the avian cranial NC cell migratory pathways during the early phase of migration (McLennan et al., 2010). Cells internalize chemoattractant in their local neighborhood (Li and Keller, 2000), thus depleting VEGF in the areas that have been populated for the longest periods of time (supplementary material Appendix S1).

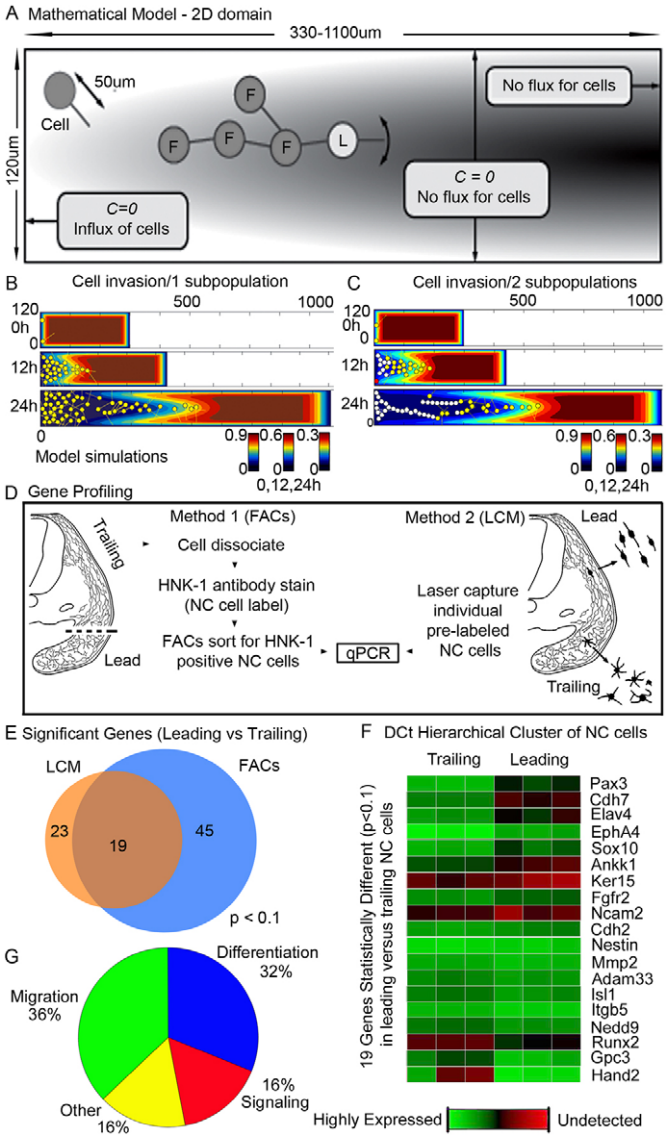

Fig. 2. The NC cell migratory stream is composed of leading and trailing cells rather than a homogeneous population. (**A**) Mathematical model schematic. (**B**) Model simulation of NC cell migration. (**C**) Model simulation of NC cell migration [two subpopulations; leaders (yellow) that respond to microenvironmental signals and trailers (red)]. Trailers that respond to directional cues from leaders turn white. (**D**) Gene profiling by FACs and LCM. (**E**) The number of genes that are significantly (P<0.1) different between leading and trailing NC cells when isolated by LCM or FACs. (**F**) DCt hierarchical cluster analysis. (**G**) The distribution of the 19 significant (P<0.1) genes displayed in F.

In our model, NC cells undergo directional movement by creating a cell-induced gradient of VEGF. This gradient is followed to the end of the migratory domain. The migratory domain itself lengthens in the x-direction, according to a logistic growth function fit to experimental measurements (supplementary material Appendix S1). Throughout the 2D domain, we assume standard logistic production of VEGF by the overlying ectoderm. However, as long as cell consumption of VEGF is more rapid than its replenishment, there is no functional change to the VEGF profile (supplementary material Appendix S1).

Simulations of our model reveal that a simple cell chemotaxis hypothesis is insufficient to explain our experimental data (Fig. 2B). That is, if we assume a homogeneous population of NC cells, we find that those cells that emerge later from the neural tube have no VEGF gradient to follow and become trapped near the entrance to the migratory pathway (Fig. 2B; supplementary material Movie 1). This problem is inherent in this mechanism of invasion, as there is always a time at which all the chemoattractant at the entrance to the migratory pathway has been consumed or degraded. After this time, there is no gradient adjacent to the neural tube to direct newly emerging cells (Fig. 2B; supplementary material Movie 1).

When we refine our model to include two NC cell subpopulations, model simulations predict most cells invade the domain in a multicellular stream (Fig. 2C; supplementary material Movie 2). That is, cells emerging early from the neural tube that form the migratory front (leading cells) detect and respond to the VEGF gradient (Fig. 2C, yellow). Later emerging cells (trailing cells) respond to directional cues from leading NC cells (Fig. 2C, red in the absence of directional cues; white once direction is found). VEGF is consumed by both leading and trailing cells. Thus, our model predicts that a heterogeneous NC cell migratory population composed of leading and trailing cells is required for successful invasion of the migratory domain.

Profiling of the NC cell migratory stream reveals distinct gene expression patterns for leading versus trailing cells

Do cells that travel long distances to targets have distinct leading and trailing cell subpopulations, shown by unique gene expression profiles, as predicted by our model? To address this question within the NC model, we analyzed the molecular profiles of leading and trailing cell subpopulations, using two separate techniques (Fig. 2D,E). Leading and trailing NC cells were isolated from dissected and dissociated tissue via HNK-1 staining (to accurately select NC cells) and sorted by FACS or isolated as single cells via laser capture microdissection (LCM). We compared the expression of 84 genes of interest based on their previously documented expression in NC cells and known involvement in NC cell delamination, migration or differentiation (supplementary material Table S1). From the NC cells sorted by FACS, 45 of the 84 genes showed significant differences in expression ($P<0.1$) comparing the leading and trailing NC cells (Fig. 2E). Using LCM, 23 out of the 84 genes showed significant differences in expression ($P<0.1$) comparing the leading and trailing NC cells (Fig. 2E). By directly comparing the LCM and FACS data, we find that 19 out of the 84 genes have significant differences with both isolation methods (Fig. 2E; supplementary material Fig. S1). Given the biological complexity and inherent variation of in vivo model systems, we define statistical significance of differential expression as $P<0.1$ when analyzed by two separate methodologies.

Our molecular profiling comparison reveals that leading NC cells have upregulated expression of distinct sets of cell guidance and cell navigation genes (Fig. 2E; supplementary material Fig. S1). These include specific cell guidance factor receptors (e.g. EphA4), integrins (e.g. Itgb5), matrix metalloproteases (e.g. MMP2) and cadherins (e.g. Cdh7) that are distinct from trailing NC cells (Fig. 2E; supplementary material Fig. S1). By contrast, trailing NC cells have upregulated expression of cadherins distinct from leading NC cells (Fig. 2E; supplementary material Fig. S1). The differences in gene expression patterns suggest that leading and trailing NC cells respond differently to local microenvironmental signals, which are related to their navigation and differentiation program. Thus, our model simulations of a heterogeneous NC cell migratory population accurately predicted the requirement for distinct leading and trailing cell behaviors, the molecular correlates of which were identified by gene profiling.

In silico and experimental results reveal that leading NC cells compensate for the loss of trailing NC cells after tissue ablation and distribute along the entire migratory pathway

Based on the above findings, we refined our initial hypothesis to enable chemotaxis to guide a heterogeneous population of NC cells to move in a directional manner to a long-distance target. Within our model, leading NC cells respond to chemotactic signals in the microenvironment and trailing NC cells respond by touch to directional signals from leaders. To test our hypothesis, we carried out a number of tissue transplantation and tissue ablation model simulations and experiments. Our gene profiling provides a distinct molecular signature for leading versus trailing NC cells such that we can analyze changes in gene expression pattern after tissue ablation or tissue transplantation to a new position within the migratory stream. Changes in the gene expression pattern of leading or trailing NC cells may then be correlated with cell behavioral changes predicted by our model.

First, we designed an experiment that ablates trailing NC cells to test whether propagation of leading cells is reliant on cell contact with trailing cells (Fig. 3A-C). Using a glass needle, we remove part of the fluorescently labeled dorsal neural tube at 10 hours after electroporation (Fig. 3B). In silico, this is achieved by ceasing to input new cells into the domain at 10 hours after the start of the simulation (Fig. 3K; supplementary material Movie 3). When the number of later emerging cells is significantly reduced, the model predicts that leading cells spread out along the length of the migratory domain and do not move as a subpopulation to the distal end of the domain (Fig. 3K; supplementary material Movie 3). This is a direct consequence of the dynamic way in which the non-ablated cells create and follow the VEGF gradient. The leading cells react to the gradient as before (Fig. 3K; supplementary material Movie 3). However, all trailing cells are ablated, so that later emerging non-ablated leading cells now explore sub-regions where the chemoattractant has not been completely depleted, closer to the edges of the migratory domain [Fig. 3K (12 hours); supplementary material Movie 3]. Thus, in silico simulations predict that NC cells distribute evenly along the migratory pathway when cell numbers are substantially reduced [Fig. 3K (24 hours); supplementary material Movie 3]. This was counter-intuitive to the anticipated outcome. We expected that when the number of later emerging cells is significantly reduced, either all leading cells would respond to the VEGF signal and invade the migratory domain, or remain near the neural tube due to the lack of population pressure.

In support of our model predictions, we find, after experimental manipulation, that leading NC cells compensate for the absence of trailing neighbors and distribute all along the migratory pathway (Fig. 3D,E; $n=7$ embryos; supplementary material Fig. S2). Leading NC cell orientation measurements reveal that cells mimic the cellular profile of a typical migratory stream (Fig. 3G; $n=168$ cells, embryos). Specifically, NC cells located closest to the neural tube lack orientation to the migratory pathway, but cell orientation is acquired downrange (Fig. 3G). Leading NC cells that invade and colonize the branchial arch display less orientation to the migratory pathway (Fig. 3G). Time-

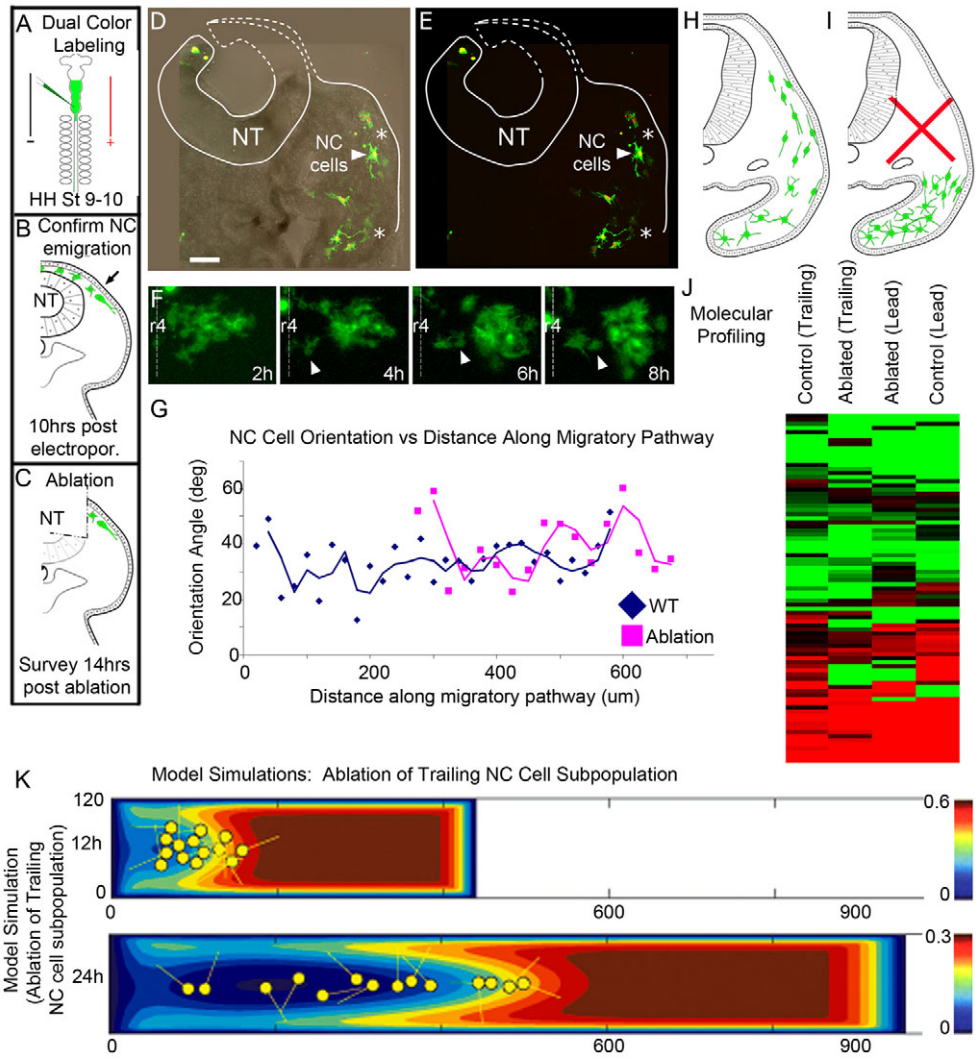

Fig. 3. Leading NC cells compensate for the loss of trailing NC cells after trailing ablation. (**A-C**) Experiment schematic. (**D**,**E**) Transverse sections after ablation (dotted line; asterisks indicate where 'lead' and 'trailing' NC cells were isolated using LCM). (**F**) Selected images from time-lapse of NC cell migration after ablation. (**G**) Average nuclear orientation angles with respect to distance along the migratory route after ablation (168 cells, seven embryos). (**H**,**I**) Possible expected outcomes after ablation. (**J**) Heat map of qPCR molecular profiles of LCM-isolated NC cells. (**K**) Model simulations after ablation. Scale bar: 50 μm. NC, neural crest cells; NT, neural tube; WT, wild type; hr, hours.

lapse confocal imaging also reveals that some leading NC cells stop in proximal positions along the migratory pathway (Fig. 3F; *n*=3 time-lapse imaging sessions), rather than migrating distally and reversing direction to fill in for missing neighbors. Thus, model predictions and experimental results agree that leading NC cells distribute all along the migratory pathway upon substantial reduction of NC cell numbers.

The distribution and cell morphologies of the leading NC cells after ablation of the trailing subpopulation suggest that some leading NC cells alter their identity from a leading to a trailing phenotype (Fig. 3H,I). To identify changes in the molecular profile of leading NC cells (after reduction in the number of trailing NC cells), we use LCM to isolate single NC cells at proximal and distal locations along the migratory pathway (Fig. 2D). Using the same 84 genes, the molecular profile of leading NC cells (after ablation of the trailing subpopulation) is similar to control leading NC cells (Fig. 3J). However, leading NC cells that remain at proximal positions along the migratory pathway are more similar to control trailing NC cells (Fig. 3J). The results are the same if only the 24 genes that are differentially expressed between the leading and trailing NC cells via LCM are used (data not shown). Thus, ablation of trailing NC cells causes leading NC cells to adapt their molecular profile and cell behaviors to mimic a typical NC cell migratory stream.

Trailing NC cells assume a leading cell gene expression profile and cell behavior after transplantation to the migratory front

To examine the equipotency of all migratory NC cells to lead, i.e. to respond to, chemotactic signals, we transplanted tissue containing the trailing NC cell subpopulation into the leading region of the migratory front (Fig. 4A-C; *n*=12 embryos; supplementary material Fig. S2). We find that the transplanted trailing NC cells invade the branchial arch, a region they usually do not encounter (Fig. 4D,E,G). We next performed LCM followed by qPCR on trailing NC cells transplanted into the migratory front. The gene expression profiles of all transplanted NC cells (those categorized before transplantation as leading and trailing) are similar to control leading NC cells (Fig. 4H). In addition, morphometric measurements show transplanted NC cells have a cell orientation profile of a typical migratory stream (Fig. 4F; *n*=200 cells). Thus, trailing NC cells alter their cellular and molecular profile to assume the leading NC cell phenotype.

We are conscious of the fact that we are using a 2D model to describe a 3D process. Therefore, our model predictions must be treated cautiously. One example in which the difference between two and three dimensions is expressly manifested is when trailing cells are transplanted to the front of a migratory stream. In silico, the VEGF from the subregion of the trailing migratory pathway is

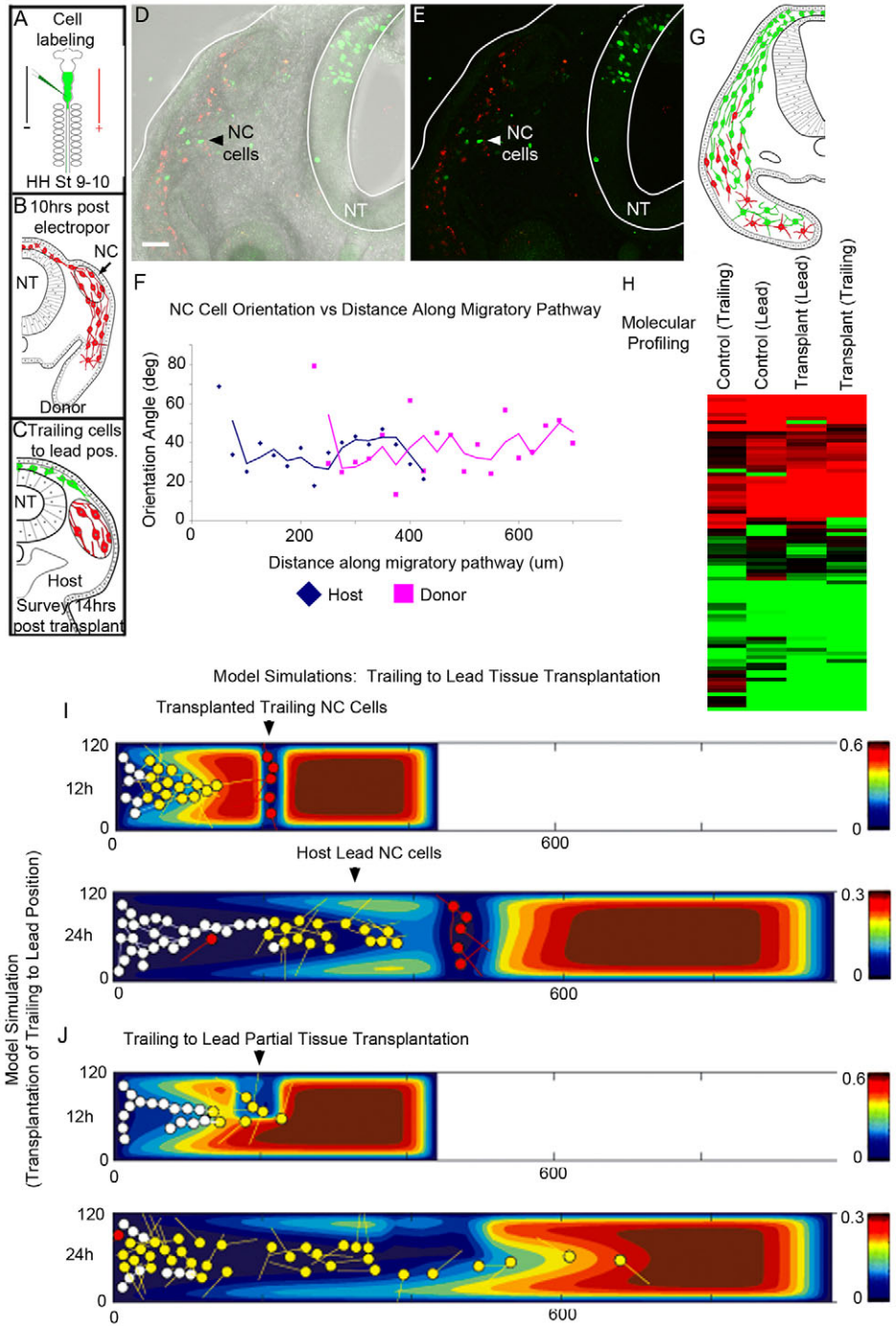

Fig. 4. Behavior and molecular profile of trailing NC cells transplanted to the leading position of the migratory stream. (**A-C**) Experimental schematic. (**D**,**E**) Transverse sections after transplantation. (**F**) Average nuclear orientation angles with respect to distance along the migratory route [72 host cells (blue), 128 donor cells (pink), 12 embryos]. (**G**) Schematic representation of cell migration after transplantation. (**H**) Heat map of qPCR molecular profiles of LCM-isolated NC cells. (**I**) Model simulation. Leaders (yellow), trailers that are following others (white) and trailers that are not following others (red). (**J**) Model simulation. Tissue transplant is half the width of the domain. Trailing cells given the ability to become leading cells. Scale bar: 50 μm. NC, neural crest cells; NT, neural tube; hr, hours.

also transplanted with the trailing cells (Fig. 4I; supplementary material Movie 4). The transplanted region has a much lower concentration of VEGF than the local microenvironment (Fig. 4I; supplementary material Movie 4). This prevents host leading cells from moving through the transplanted region, as the VEGF gradient is unfavorable (Fig. 4I; supplementary material Movie 4). In our 2D domain, cells become trapped proximal to the transplant (Fig. 4I; supplementary material Movie 4). Transplanted trailing NC cells respond to leading NC cells and therefore also fail to migrate (Fig. 4I; supplementary material Movie 4).

Owing to the inconsistency between our experimental and theoretical results, we re-evaluate the parameters used in silico to better reflect the experimental approach. In vivo, migratory NC cells are able to move in three dimensions and around the tissue transplant site. In silico, our initial simulated tissue transplant spanned the entire width of the domain (Fig. 4I; supplementary material Movie 4) and hence all migratory cells have to move through the transplant. To make the two approaches more cohesive, the in silico transplant was reduced to half the width of the domain (Fig. 4J; supplementary material Movie 5). In this way, trailing cells in silico are able to sample the VEGF in a number of directions. Furthermore, we gave trailing cells the ability to convert to a leading cell behavior if the VEGF gradient is favorable in a large enough proportion of these directions. With these changes, migratory cells now efficiently migrate from and beyond the transplant site to follow the endogenous VEGF along the domain

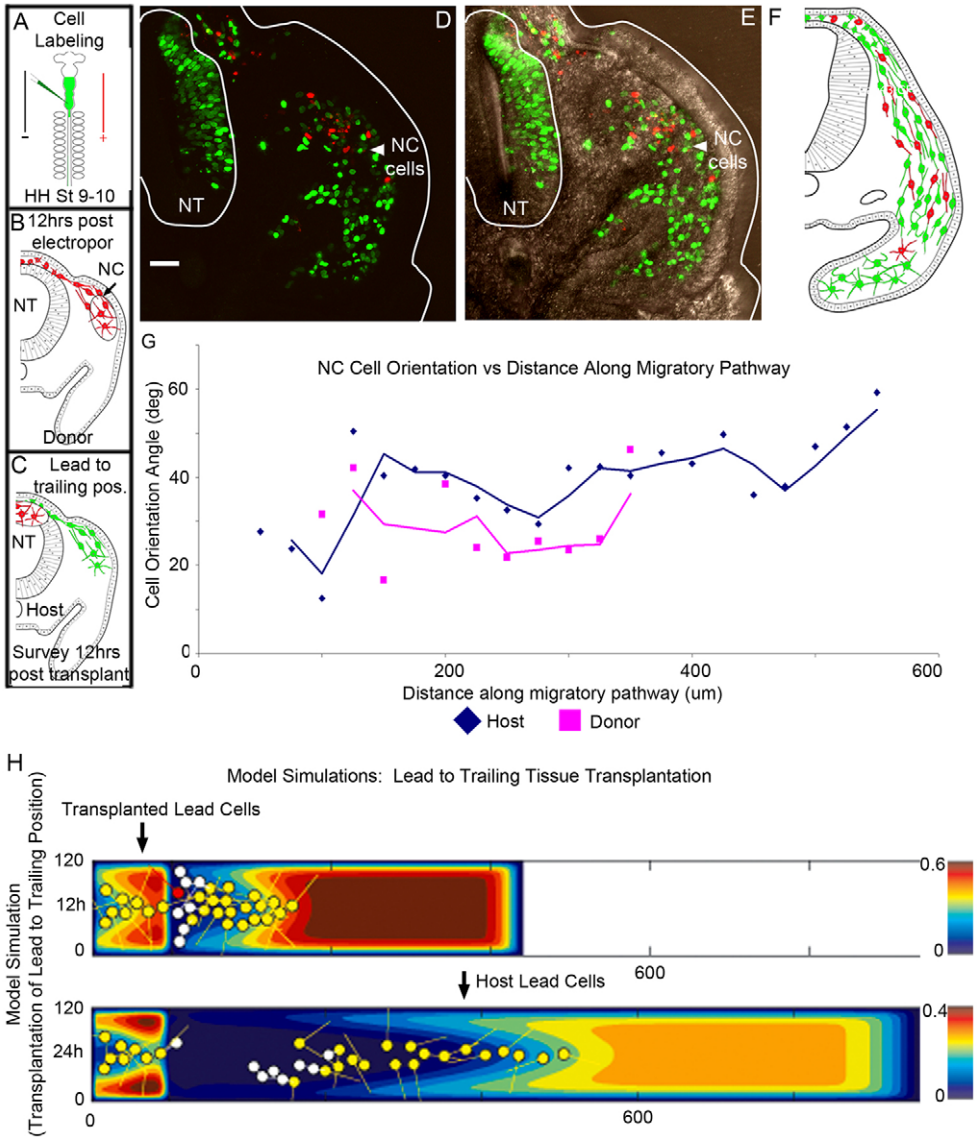

Fig. 5. Very few leading NC cells migrate after leading to trailing transplant. (**A-C**) Experiment schematic. (**D**,**E**) Transverse sections after tissue transplantation, also represented schematically (**F**). (**G**) Average nuclear orientation angles after trailing NC cell ablation [169 host cells (blue), 37 donor cells (pink), 3/13 embryos]. (**H**) Model simulation. Leaders (yellow), trailers that are following others (white) and trailers that are not following others (red). Scale bar: 50 μm. NC, neural crest cells; NT, neural tube; hr, hours.

in silico, which is consistent with the experimental result (Fig. 4J; supplementary material Movie 5). Thus, by adapting the model to more accurately reflect cell behaviors in three dimensions, our model predicts that a cell-induced gradient and two subpopulations of NC cells is consistent with experimental results.

Model predictions and experiment both reveal that leading NC cells transplanted into proximal stream positions remain in proximal positions and do not invade the distal target

To test the ability of leading NC cells to respond to signals within proximal positions of the migratory stream, we transplanted a subregion of the migratory front to the dorsal neural tube, proximal to the host leading NC cells (Fig. 5A-C; n=13 embryos, supplementary material Fig. S2). In order to simulate this in the model, we inserted a subpopulation of cells into the 2D rectangular domain at x=0 (Fig. 5H; supplementary material Movie 6). As with the previous experiment, we assume that VEGF is transplanted with the cells (Fig. 5H; supplementary material Movie 5), as the overlying ectoderm of the sub-region is also transplanted. In this scenario, the donor and host embryos are at the same developmental stage, so that the VEGF levels are assumed of the same order of magnitude (Fig. 5H). However, as the donor sub-region is removed from the migratory front, it is an area in which the VEGF is not depleted. Conversely, the VEGF levels within the proximal subregion of the host migratory stream are reduced to negligible levels. Hence, the cells in the transplanted tissue experience a more favorable chemoattractant-rich microenvironment and cells do not emerge from the neural tube (Fig. 5H; supplementary material Movie 5).

In this experiment, we transplant leading NC cells into the neural tube during the time when trailing NC cells emerge from the neural tube (Fig. 5C; n=13 embryos). The cellular profile of the migratory stream in this experiment is more challenging to determine as we find that fewer NC cells migrate away from the transplant site (Fig. 5D-F; n=206 cells), in agreement with our model predictions. Specifically, we find that transplanted NC cells do not migrate to the front of the migratory stream (Fig. 5D-G). Rather, transplanted NC cells integrate into the trailing region of the migratory stream (Fig. 5D-G). Thus, in silico and experimental results are in agreement that leading NC cells transplanted into proximal stream positions do not move rapidly to resume their position as leading cells, but remain in proximal positions.

DISCUSSION

A cell-induced gradient model of long distance cell migration

We used an integrative theoretical and experimental approach to test our hypothesis that chemotaxis drives a population of cells to move in a directional manner to a long-distance target. We examined this hypothesis in the embryonic NC cell migratory population model. Our model predicted that successful long distance NC cell migration requires two cell types: leading cells that respond to a chemoattractant gradient and trailing cells that are guided by the leading cells via cell-cell contact (Figs 2, 5). The existence of two distinct NC cell subpopulations within a typical migratory stream, characterized by unique gene expression patterns that correlate with cell behavioral differences, was confirmed by gene expression profiling (Fig. 2). Gene expression profiling using a novel qPCR technique to analyze small numbers of cells extracted by laser microdissection determined unique cell guidance and cell navigation signatures of leading versus trailing NC cells (Figs 3, 6). Although we cannot rule out that there is a spectrum of cellular phenotypes from front-to-back in a migratory stream (rather than a binary choice of leading or trailing cell), further studies that sequentially extract and profile cells from front-to-back within a migratory stream will provide crucial data for our model and help address this.

Our theoretical model made a number of predictions of experimental manipulations which were shown to be true. First, model simulations predicted that leading NC cells distribute all along the migratory pathway in the absence of trailing NC cells (Fig. 3). Experimental results confirmed this outcome and revealed that leading NC cells developed a leading and trailing gene expression profile depending on cell position within the migratory stream (Fig. 3). Second, our model predicted that trailing NC cells altered their behavior and responded to chemotactic signals when moved to the migratory front (Fig. 4). Experimental results confirmed trailing cells altered their gene expression profile and cell orientation to leading cells, when transplanted to the migratory front (Fig. 4). Third, leading NC cells did not invade distal targets when moved into the proximal region of the migratory stream (Fig. 5). This phenotype was confirmed by experiment (Fig. 5).

The success of our model motivates further experimental study. For example, the mechanisms that regulate differences in leading versus trailing NC cell gene expression patterns and how this is directly correlated with changes in cell behaviors, are yet to be discovered. One interesting possibility is that later emerging NC cells may exit the neural tube with a gene expression pattern comparable with the leading NC cell phenotype. However, these cells may then convert to a trailing NC cell phenotype in the absence of sensing a chemotactic signal. This change in cell behavior is predicted by our theoretical model (Fig. 2). In this scenario, the rate of chemotactic production, dilution and consumption controls the size of the leading NC cell subpopulation.

Alternatively, leading NC cells may play a direct role in regulating later emerging NC cells to adopt a trailing cell phenotype. For example, leading NC cells may directly inhibit a leading cell phenotype in later emerging cells. This type of mechanism has been suggested from studies of collective cell migration during angiogenesis (Tammela et al., 2011). During angiogenesis, vessel sprouting consists of tip and stalk cells that have distinct gene expression profiles (Eilken and Adams, 2010). The proper ratio between tip and stalk cells is required for correct blood vessel sprouting and branching patterns (Eilken and Adams, 2010). When Notch signaling is blocked, stalk cells adopt a tip phenotype and display excessive sprouting (Hellström et al., 2007; Suchting et al., 2007; Siekmann and Lawson, 2007). This revealed a mechanism by which Notch signaling inhibits the tip cell phenotype in trailing stalk cells. Whether leading NC cells play a similar role is not known. NC cells tend to maintain a spatial migratory order and not exchange leading and trailing cell positions (Kulesa et al., 2008), such that this type of inhibitory mechanism is plausible. In addition, a mechanism that would inhibit trailing NC cells from adopting a leading cell phenotype would prevent bifurcation of the migratory stream into separate branches behind the migratory front.

In summary, we suggest that long-distance NC cell migration is driven by a two-component mechanism that includes chemotaxis and cell-cell contact (Fig. 6). As a result of analyzing our model, we predict that early emerging NC cells use a cell-induced gradient mechanism to move in a directional manner over long distances to a target site (Fig. 6). We predict that later emerging NC cells

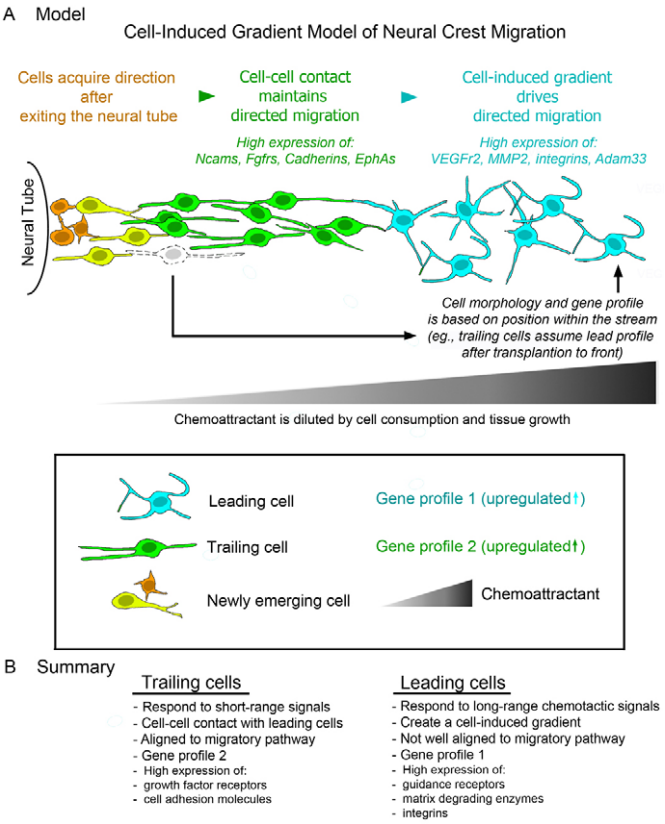

Fig. 6. Neural crest cell migration: a cell-induced chemotaxis model. (**A**) NC cells exit the NT without orientation to the migratory pathway (orange cells), but rapidly acquire direction (yellow cells). Leading NC cells (blue) respond to long-range chemotactic signals, including VEGF. Leading cells spread out from the migratory pathway and have a distinct gene profile that is navigation oriented. Trailing NC cells (green) respond to short-range signals for guidance information from other local migratory NC cells. Trailing NC cells are highly aligned with the migratory pathway and have a distinct gene profile that is cell-cell contact oriented. Ablation and tissue transplantation studies, demonstrate that both trailing and leading NC cells have a high degree of plasticity. Key shows the NC cell types and gene profiles of leading and trailing cells. (**B**) Summary details differences in the features of the leading and trailing NC cells.

require a mechanism of invasion other than chemotaxis, and use cell-cell contact to follow leading cells (Fig. 6). Thus, leading cells respond to long-range signals and trailing cells to short-range cues to maintain a directed multicellular stream (Fig. 6).

Future experiments that include gain- and loss-of-function of particular genes expressed differently in leading and trailing NC cell subpopulations will help to identify the factors crucial for cell guidance and maintenance of a NC cell migratory stream. We suggest that our closely linked, combined theoretical and experimental framework offers a powerful approach for integrating multiscale biological data and a means to robustly test model hypotheses. Our results fill a major void in the current understanding of long-distance cell migration and offer mechanistic insights that have direct application to model systems in development and cancer.

Acknowledgements
We thank Andrew Box and Jeff Haug for their assistance with cytometry analysis; William McDowell for help with qPCR; Karen Smith, Nancy Thomas, Nannette March and Sharon Beckham for assistance with Histology; and Hua Li and Linghui Li for their help with bioinformatics analysis.

Funding
P.M.K. acknowledges funding from the National Institutes of Health [1R01HD057922] and the Stowers Institute for Medical Research. P.K.M. was partially supported by a Royal Society Wolfram Research Merit Award. Deposited in PMC for release after 12 months.

Competing interests statement
The authors declare no competing financial interests.

Supplementary material
Supplementary material available online at
http://dev.biologists.org/lookup/suppl/doi:10.1242/dev.081471/-/DC1

References
Abercrombie, M. (1979). Contact inhibition and malignancy. *Nature* **281**, 259-262.
Aman, A. and Piotrowski, T. (2010). Cell migration during morphogenesis. *Dev. Biol.* **341**, 20-33.
Burns, T. C. and Steinberg, G. K. (2011). Stem cells and stroke: opportunities, challenges and strategies. *Expert Opin. Biol. Ther.* **11**, 447-461.
Cai, H., Huang, C. H., Devreotes, P. N. and Iijima, M. (2012). Analysis of chemotaxis in Dictyostelium. *Methods Mol. Biol.* **757**, 451-468.
Carmona-Fontaine, C., Matthews, H. K., Kuriyama, S., Moreno, M., Dunn, G. A., Parsons, M., Stern, C. D. and Mayor, R. (2008). Contact inhibition of locomotion in vivo controls neural crest directional migration. *Nature* **456**, 957-961.
Darnton, N. C., Turner, L., Rojevsky, S. and Berg, H. C. (2010). Dynamics of bacterial swarming. *Biophys. J.* **98**, 2082-2090.
Davis, E. M. and Trinkaus, J. P. (1981). Significance of cell-to cell contacts for the directional movement of neural crest cells within a hydrated collagen lattice. *J. Embryol. Exp. Morphol.* **63**, 29-51.
Dormann, D. and Weijer, C. J. (2003). Chemotactic cell movement during development. *Curr. Opin. Genet. Dev.* **13**, 358-364.
Druckenbrod, N. R. and Epstein, M. L. (2007). Behavior of enteric neural crest-derived cells varies with respect to the migratory wavefront. *Dev. Dyn.* **236**, 84-92.
Eilken, H. M. and Adams, R. H. (2010). Dynamics of endothelial cell behavior in sprouting angiogenesis. *Curr. Opin. Cell Biol.* **22**, 617-625.
Friedl, P. and Gilmour, D. (2009). Collective cell migration in morphogenesis, regeneration and cancer. *Nat. Rev. Mol. Cell Biol.* **10**, 445-457.
Gammill, L. S. and Roffers-Agarwal, J. (2010). Division of labor during trunk neural crest development. *Dev. Biol.* **344**, 555-565.
Hamburger, V. and Hamilton, H. L. (1951). A series of normal stages of development of the chick embryo. *J. Morphol.* **88**, 49-92.
Hatten, M. E. and Roussel, M. F. (2011). Development and cancer of the cerebellum. *Trends Neurosci.* **34**, 134-142.
Hellström, M., Phng, L. K., Hofmann, J. J., Wallgard, E., Coultas, L., Lindblom, P., Alva, J., Nilsson, A. K., Karlsson, L., Gaiano, N. et al. (2007). Dll4 signalling through Notch1 regulates formation of tip cells during angiogenesis. *Nature* **445**, 776-780.
Huang, Z. (2009). Molecular regulation of neuronal migration during neocortical development. *Mol. Cell. Neurosci.* **42**, 11-22.
Jiang, M., Stanke, J. and Lahti, J. M. (2011). The connections between neural crest development and neuroblastoma. *Curr. Top. Dev. Biol.* **94**, 77-127.
Kasemeier-Kulesa, J. C., Teddy, J. M., Postovit, L. M., Seftor, E. A., Seftor, R. E., Hendrix, M. J. and Kulesa, P. M. (2008). Reprogramming multipotent tumor cells with the embryonic neural crest microenvironment. *Dev. Dyn.* **237**, 2657-2666.
Kulesa, P. M. and Gammill, L. S. (2010). Neural crest migration: patterns, phases and signals. *Dev. Biol.* **344**, 566-568.
Kulesa, P. M., Teddy, J. M., Stark, D. A., Smith, S. E. and McLennan, R. (2008). Neural crest invasion is a spatially-ordered progression into the head with higher cell proliferation at the migratory front as revealed by the photoactivatable protein, KikGR. *Dev. Biol.* **316**, 275-287.
Kulesa, P. M., Bailey, C. M., Kasemeier-Kulesa, J. C. and McLennan, R. (2010). Cranial neural crest migration: new rules for an old road. *Dev. Biol.* **344**, 543-554.
Li, W. and Keller, G. (2000). VEGF nuclear accumulation correlates with phenotypical changes in endothelial cells. *J. Cell Sci.* **113**, 1525-1534.
McLennan, R. and Kulesa, P. M. (2007). In vivo analysis reveals a critical role for neuropilin-1 in cranial neural crest cell migration in chick. *Dev. Biol.* **301**, 227-239.
McLennan, R. and Kulesa, P. M. (2010). Neuropilin-1 interacts with the second branchial arch microenvironment to mediate chick neural crest cell dynamics. *Dev. Dyn.* **239**, 1664-1673.
McLennan, R., Teddy, J. M., Kasemeier-Kulesa, J. C., Romine, M. H. and Kulesa, P. M. (2010). Vascular endothelial growth factor (VEGF) regulates cranial neural crest migration in vivo. *Dev. Biol.* **339**, 114-125.
Murase, S. and Horwitz, A. F. (2004). Directions in cell migration along the rostral migratory stream: the pathway for migration in the brain. *Curr. Top. Dev. Biol.* **61**, 135-152.
Noden, D. M. and Trainor, P. A. (2005). Relations and interactions between cranial mesoderm and neural crest populations. *J. Anat.* **207**, 575-601.
Perris, R. and Perissinotto, D. (2000). Role of the extracellular matrix during neural crest cell migration. *Mech. Dev.* **95**, 3-21.
Richardson, B. E. and Lehmann, R. (2010). Mechanisms guiding primordial germ cell migration: strategies from different organisms. *Nat. Rev. Mol. Cell Biol.* **11**, 37-49.
Roussos, E. T., Condeelis, J. S. and Patsialou, A. (2011). Chemotaxis in cancer. *Nat. Rev. Cancer* **11**, 573-587.
Sauka-Spengler, T. and Bronner-Fraser, M. (2008). Evolution of the neural crest viewed from a gene regulatory perspective. *Genesis* **46**, 673-682.
Siekmann, A. F. and Lawson, N. D. (2007). Notch signalling limits angiogenic cell behaviour in developing zebrafish arteries. *Nature* **445**, 781-784.
Streichan, S. J., Valentin, G., Gilmour, D. and Hufnagel, L. (2011). Collective cell migration guided by dynamically maintained gradients. *Phys. Biol.* **8**, 045004.
Suchting, S., Freitas, C., le Noble, F., Benedito, R., Bréant, C., Duarte, A. and Eichmann, A. (2007). The Notch ligand Delta-like 4 negatively regulates endothelial tip cell formation and vessel branching. *Proc. Natl. Acad. Sci. USA* **104**, 3225-3230.
Tammela, T., Zarkada, G., Nurmi, H., Jakobsson, L., Heinolainen, K., Tvorogov, D., Zheng, W., Franco, C. A., Murtomäki, A., Aranda, E. et al. (2011). VEGFR-3 controls tip to stalk conversion at vessel fusion sites by reinforcing Notch signalling. *Nat. Cell Biol.* **13**, 1202-1213.
Tarbashevich, K. and Raz, E. (2010). The nuts and bolts of germ-cell migration. *Curr. Opin. Cell Biol.* **22**, 715-721.
Teddy, J. M. and Kulesa, P. M. (2004). In vivo evidence for short- and long-range cell communication in cranial neural crest cells. *Development* **131**, 6141-6151.
Theveneau, E. and Mayor, R. (2011). Collective cell migration of the cephalic neural crest: the art of integrating information. *Genesis* **49**, 164-176.
Trainor, P. A. (2005). Specification and patterning of neural crest cells during craniofacial development. *Brain Behav. Evol.* **66**, 266-280.
Valentin, G., Haas, P. and Gilmour, D. (2007). The chemokine SDF1a coordinates tissue migration through the spatially restricted activation of Cxcr7 and Cxcr4b. *Curr. Biol.* **17**, 1026-1031.
Young, H. M., Bergner, A. J., Anderson, R. B., Enomoto, H., Milbrandt, J., Newgreen, D. F. and Whitington, P. M. (2004). Dynamics of neural crest-derived cell migration in the embryonic mouse gut. *Dev. Biol.* **270**, 455-473.

Supplementary Material: Mathematical Model

1 Domain growth

In vivo, the domain of migration grows along the x axis, so that the length of the domain increases from 330μm initially to reach 1100μm at 24hrs into migration. This is a huge increase, and may have a large impact on the methods and success of migration. As such, domain growth is included in the model. The cells move with the underlying domain, and growth also impacts on the levels of chemoattractant. To solve numerically, it was necessary to rescale the equations by $z = x/L$, so that the equations are mapped onto a stationary domain. The solutions are then rescaled back to the moving domain for viewing.

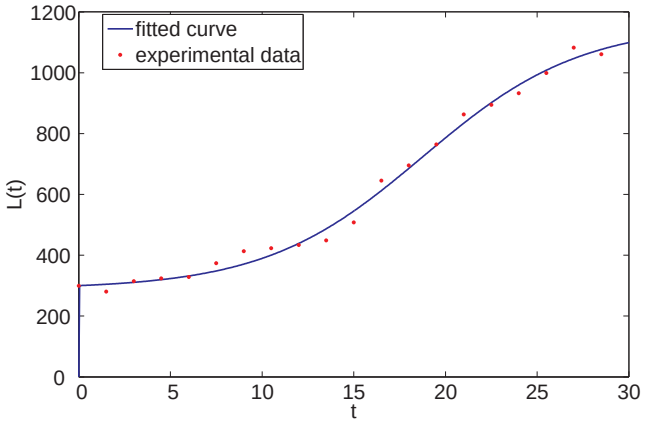

Figure 1: Experimental data (red dots) for domain length and the fitted logistic form (blue line).

The domain growth is found by fitting a logistic curve of the form

$$L(t) = \left(\frac{L_\infty e^{L_\infty \alpha (t-t_s)}}{L_\infty - 1 + e^{L_\infty \alpha (t-t_s)}} + 1 - \frac{L_\infty e^{L_\infty \alpha (-t_s)}}{L_\infty - 1 + e^{L_\infty \alpha (-t_s)}} \right) W, \tag{1}$$

where $L(t)$ is the length of the domain and W is the initial width of the domain, to experimental data. This gives $L_\infty = 960$, $\alpha = 0.0580$ and $t_s = -16$ (see Figure 1).

2 Chemoattractant

From data in the chick embryo, VEGF is expressed in the chick surface ectoderm directly overlying the NC cell migratory pathway and has been shown to be a NC cell chemoattractant (McLennan et al., 2010). We assume a constant production of VEGF by the ectoderm cells throughout the domain of invasion. To reconcile this constant production with our hypothesis of chemotaxis as a mechanism for invasion, we postulate that the cells may create their own gradient of chemoattractant through the internalization of VEGF. This would lead to lower levels of VEGF in areas where the cells have been present for longer periods, so that there is more VEGF further away from the neural tube. In our model, VEGF is produced logistically throughout the region (with linear proliferation rate, χ), and the internalization of VEGF by cells is modelled by weighted sink terms around the cells.

Hence the rate of change of VEGF concentration, c, is given by

$$\frac{\partial c}{\partial t} = \overbrace{D_c\left(\frac{1}{L^2}\frac{\partial^2 c}{\partial \xi^2} + \frac{\partial^2 c}{\partial y^2}\right)}^{\text{Diffusion}} \overbrace{-\lambda \sum_{i=1}^{n} c(x,y)\exp\left[-d\left((x-x_i)^2+(y-y_i)^2\right)\right]}^{\text{internalization}} \overbrace{-\frac{L'}{L}c}^{\text{Dilution}} + \overbrace{\chi c(1-c)}^{\text{Production}},$$

where D_c is the diffusion coefficient for the VEGF and λ and d are parameters governing the height and width of the weighting function used to describe the consumption of chemoattractant. We assume VEGF is produced logistically with a rate χ, however our results are not sensitive to this parameters as long as it is not large enough to overwhelm the consumption by cells (see Figure 2). There are n cells in the domain, which is $w\mu$m wide and $h\mu$m high, and the ith cell center is at (x_i, y_i).

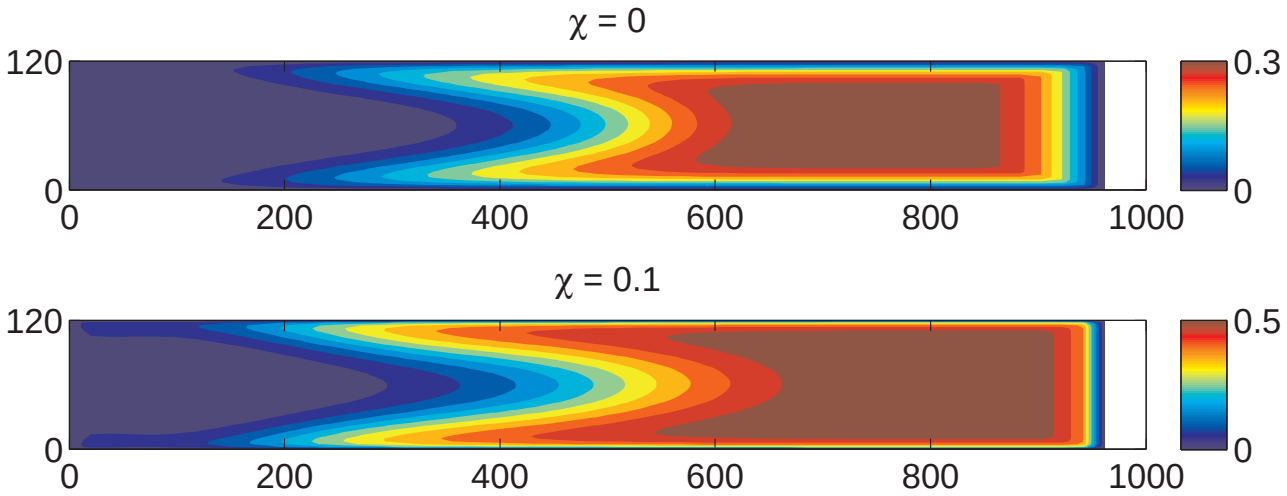

Figure 2: Simulated VEGF concentration with $\chi = 0$ and $\chi = 0.1$ after 24hrs.

We take as boundary conditions that the VEGF concentration is zero at each of the four boundaries of the region. This ensures that the concentration is not artificially high there due to the lower consumption of VEGF close to the edges of the domain (since there will be more overlapping regions of cell consumption in the interior of the domain). Hence the cells will not artificially cluster at the edge of the domain. We note in addition that this also provides a way of artificially simulating the exclusion zones between the migrating streams without explicitly including the inhibitory factors that may be present in these regions.

The concentration of VEGF may then be solved at each time step using the NAG solver d03ra. The zero boundary conditions require some care, however, to ensure that the initial conditions are sufficiently smooth to be able to solve the resultant equations.

Table S1. Taqman assay IDs for all genes analyzed by qPCR

Gene	Assay ID/Part number
ADAM10	Gg03364319_m1
ADAM33	Gg03361516_m1
ANKK1	Gg03644038_m1
BAMBI	AJS065I
BMPR1A	Gg03339693_m1
BMPR1B	Gg03366638_m1
BMPR2	Gg03345679_m1
CCL19	Gg03321902_m1
CCR7	AJCSUTO
CCR9	Gg03360247_s1
CDH11	Gg03346205_m1
CDH2	Gg03345814_m1
CDH6	Gg03345958_m1
CDH7	Gg03363795_m1
CFC1B	Gg03338500_m1
COL2A1	Gg03365340_m1
CTNNB1	Gg03348503_m1
CXCL12	Gg03365914_m1
CXCL13	AJGJPCE
CXCL8	Gg03349360_m1
CXCR1	Gg03813372_s1
CXCR4	AI5IOS0
CXCR5	Gg03344612_s1
DLX5	Gg03363550_m1
EDNRA	Gg03363278_m1
EFNB2	Gg03338769_m1
ELAV4	Gg03338811_m1
EphA2	AIMSF5V
EphA3	Gg03340036_m1
EphA4	Gg03371260_m1
EphB1	Gg03320093_m1
EphB2	Gg03349515_m1
EphB3	Gg03320080_m1
FGFR1	Gg03340352_m1
FGFR2	Gg03349085_m1
FGFR3	Gg03340332_m1
FoxD3	Gg03815041_s1
FZD7	Gg03814026_s1
GAPDH	Gg03346982_m1
GPC3	AJLJH36
HAND2	Gg03347768_m1
ISL1	Gg03339945_m1
ITGA1	Gg03366240_m1
ITGA4	Gg03320337_m1
ITGA6	Gg03348770_m1
ITGA9	Gg03342773_m1
ITGAV	Gg03371423_m1
ITGB1	Gg03357875_m1

ITGB3	Gg03346999_m1
ITGB5	Gg03365690_m1
JAG1	Gg03332179_m1
keratin15	Gg03345598_m1
keratin19	Gg03348102_m1
MBP	Gg03367316_m1
MITF	Gg03348224_m1
MMP2	Gg03365286_m1
MMP9	Gg03338321_m1
MSX1	Gg03349356_m1
NCAM2	AJS062L
Nedd9	Gg03310488_m1
NEFM	Gg03361912_m1
NESTN	Gg03348251_m1
NeuroG2	Gg03814822_s1
Notch1	Gg03317671_m1
Nrp1	Gg03371276_m1
Nrp2	Gg03364413_m1
Pax3	Gg03364367_m1
PCDH1	Gg03360150_m1
PCDH10	Gg03349770_m1
PCDH19	Gg03361701_m1
PDGFRL	Gg03328159_m1
RhoB	Gg03339342_s1
RUNX2	Gg03363363_m1
Slit2	Gg03310613_m1
Slug	Gg03333502_m1
Snail1	Gg03366757_m1
Sox10	Gg03371326_m1
Sox9	Gg03364395_m1
TFAP2A	Gg03366419_m1
TGFBR1	Gg03364206_m1
TH	Gg03338713_m1
UNC5B	Gg03352386_m1
VEGFR2	Gg03346169_m1
WISP1	Gg03343963_m1
18S	4352930E